

An optofluidic system with volume measurement and surface plasmon resonance sensor for continuous glucose monitoring

Dachao Li,^{1,a)} Bingyu Lu,¹ Rui Zhu,¹ Haixia Yu,² and Kexin Xu¹

¹State Key Laboratory of Precision Measuring Technology and Instruments,
Tianjin University, Tianjin, China

²Tianjin Key Laboratory of Biomedical Detecting Techniques and Instruments,
Tianjin University, Tianjin, China

(Received 31 October 2015; accepted 16 February 2016; published online 26 February 2016)

The traditional technology of glucose monitoring is painful and invasive because of the frequent blood collection. Nowadays, the enzyme electrode sensor is mainly used for continuous glucose monitoring in clinic, but it has inherent disadvantages of significant signal drift of current due to bioelectricity in body and the missing of hypoglycemia resulting from the irreversible consumption of glucose at the process of enzyme catalytic reaction. Interstitial fluid (ISF) transdermal extraction can be nearly unsensible which effectively reduces the pain caused by invasive detection so that it may provide a new way to monitor glucose. MEMS technology has been used to produce devices for transdermal ISF extraction, but there is a lack of on-chip ISF volume measurement capabilities, which are required to compensate skin permeability variations. This paper presents a lab-on-a-chip system for ISF transdermal extraction, ISF volume measurement, and optical glucose sensing towards the application of continuous glucose monitoring. The device significantly incorporates a MEMS volume sensor, which measures extracted ISF volume via conductance monitoring, and integrates a fiber-optic surface plasmon resonance sensor to measure glucose concentration in microchannel. The fiber-based technique provides an excellent approach to overcome the above two drawbacks of the enzyme electrode based glucose sensing. Six different volumes were tested, and the standard deviation of every sample is less than $0.05 \mu\text{l}$. The resonance wavelength moves from 549.081 nm to 592.914 nm while the concentration ranges from 0 to 200 mg/dl. The feasibility of the single-chip device for accurate and continuous monitoring of subcutaneous ISF glucose concentrations is verified. © 2016 AIP Publishing LLC. [<http://dx.doi.org/10.1063/1.4942946>]

I. INTRODUCTION

Diabetes is a global epidemic forcing millions of people to regularly measure their blood glucose levels. Current blood-based glucose monitoring technologies are invasive and painful, creating a strong demand for alternative measurement techniques. One promising candidate quantifies the glucose concentration of interstitial fluid (ISF). Continuous glucose monitoring of ISF in subcutaneous tissue allows timely detection and correction of abnormal blood glucose excursions. To date, the method for continuous glucose monitoring in ISF that has been used in clinical treatment essentially comprises biosensors based on enzyme electrode,¹⁻⁴ and the most representative products include Paradigm[®] Real-Time (Medtronic, Inc.)⁵ and FreeStyle Navigator[®] (Abbott Laboratories).⁶ These devices determine the concentration of blood glucose by detecting the glucose molecule in the ISF which is minimally invasive, practical and provides a quick response. However, these implantable biosensors based on enzyme electrode

^{a)}Electronic mail: dchli@tju.edu.cn. Tel.: +86-22-27403916.

work by the electric current monitoring of the glucose oxidation catalyzed by the oxidase immobilized on the sensor. Thus, they are susceptible to the bioelectricity in the viable tissues, which can cause a significant drift in the measuring signal, making them inappropriate for long-term monitoring. Additionally, the glucose will be consumed irreversibly because of the oxidation, resulting in an inaccuracy at low glucose concentration. Consequently, the glucose concentration of diabetics provided by these biosensors is always inaccurate, and it is necessary to calibrate periodically using finger-prick blood extraction, which brings pains like the traditional method. Especially, it is almost impossible to find hypoglycemic states in the clinical treatment of diabetes by using such implantable enzyme electrode sensors.

The drawbacks of implantable enzyme electrode sensors for continuous glucose monitoring could be effectively overcome by measuring glucose concentrations in transdermally extracted ISF samples, which have been showed to have good correlation with blood glucose concentrations.⁷ MEMS technology has been used to produce miniaturized devices for transdermal ISF extraction⁸ recently, but there is a lack of on-chip ISF volume measurement capabilities, which are required to compensate for skin permeability variations over time.⁹ Also, integration of transdermal ISF extraction and glucose sensing within a single MEMS device has yet to be realized till now. Here, we address these limitations by integrating ISF transdermal extraction, ISF volume measurement via conductance monitoring, and glucose concentration detection via fiber surface plasmon resonance (SPR) sensor in a single chip device. The microfluidic chip was utilized to extract and dilute the ISF which was scattered on the skin surface as tiny drops by mixing saline with fixed volume for easy collection of ISF extracted transdermally. But the glucose concentration decreased significantly after dilution which brings challenge of low concentration (approximately 2 mg/dl) detection. The fiber-based technique provides an excellent approach to fabricate miniaturized SPR sensors that can be integrated into the microfluidic chip to measure glucose with high sensitivity. The feasibility of the single-chip device proposed in this paper to extract ISF, measure ISF volume, continuously monitor glucose is verified. It brings out a novel method for continuous glucose monitoring in clinics.

II. STRUCTURE OF OPTICAL LAB-ON-CHIP SYSTEM

A schematic diagram of the lab-on-a-chip system is shown in Figure 1(a) which including the microfluidic chip for ISF extraction and the fiber SPR sensor for glucose monitoring. The microfluidic chip consists of a Venturi to provide driving force for ISF extraction and fluid manipulation, pneumatic valves to sequentially control the ISF extraction and collection processes, fluid chambers for the storage of ISF extracted and collected, and interconnecting micro channels. One additional pressure pump was connected with the venturi. The venturi produced negative pressure to drive the whole microfluidics system. In the normal saline injection step, in which the fluid follows the route indicating by red arrows in Figure 1(a), a volume sensor is utilized to control the input volume of normal saline, which is stored in the normal saline chamber (diameter: 2 mm) and required to mix with the transdermally extracted ISF and form a manipulable volume of fluid for easy collection that finally resulting in dilution of ISF. In the ISF collection step, in which the fluid follows the route indicating by blue arrows in Figure 1(a), the ISF and normal saline are mixed in the extraction chamber (diameter: 3 mm). Then the volume sensor is utilized to measure the diluted ISF volume again so that the volume of ISF transdermally extracted is obtained. After the ISF is extracted and diluted by the microfluidic chip, it is transported to the fiber SPR sensor inside the microchannel. Then the SPR sensor detects the glucose concentration via monitoring refractive index of the ISF dilution. The collection chamber (diameter: 2 mm) is used for waste collection. Finally, the glucose concentration in ISF is obtained using the concentrations in ISF dilution, both the volumes of saline and ISF dilution. Accordingly, the device proposed in this paper achieved ISF extraction, accurate volume measurement, and glucose monitoring. The photograph of the optical lab on chip (LOC) system is shown in Figure 1(b).

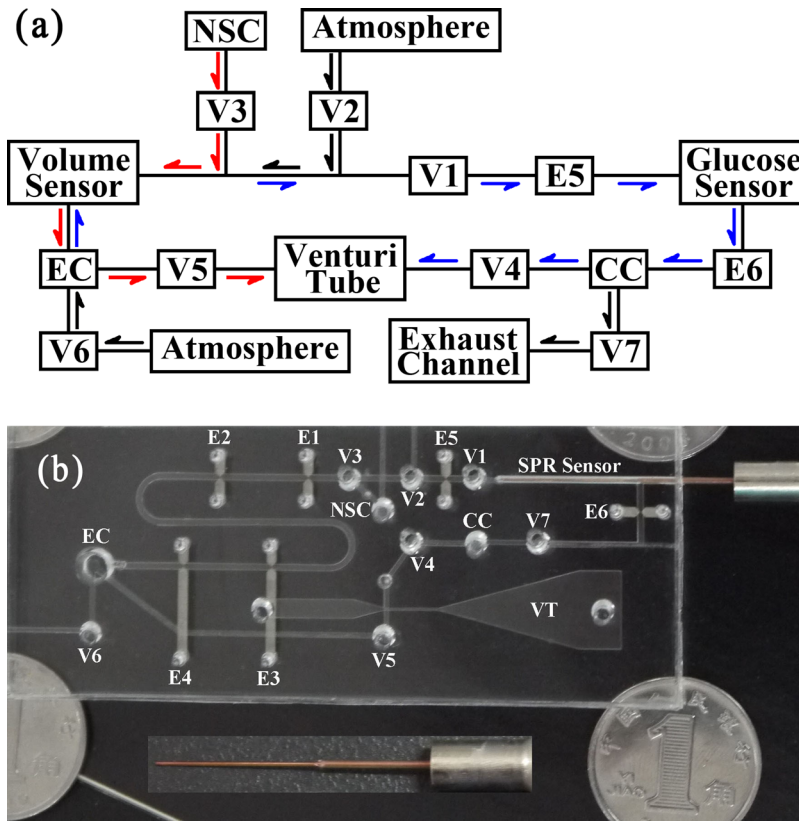


FIG. 1. (a) Schematic diagram of the lab-on-a-chip system. V1–V7 are pneumatic valves. E5 and E6 are two pairs of electrodes. EC: Extraction Chamber, NSC: Normal Saline Chamber, CC: Collection Chamber. (b) Schematic of the fiber-optic SPR sensor for glucose concentration measurement.

III. DESIGN AND FABRICATION OF VOLUME SENSOR IN MICROFLUIDIC CHIP

A. Structure design of volume sensor

The volume sensor, shown schematically in Figure 2, consists of four pairs of electrodes with tips separated by a narrow gap situated along an S-shape microchannel. Briefly, utilizing the conductivity of the electrolytic fluid (e.g., normal saline, ISF), the volume sensor controls

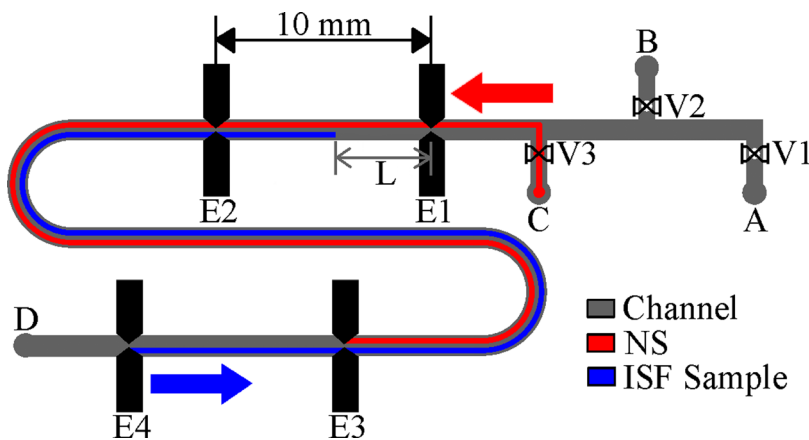


FIG. 2. Schematic of the volume sensor for controlling the input volume of normal saline for easy collection of ISF and measuring the volume of ISF. A: Collection Chamber, B: Port to Atmosphere, C: Normal Saline Chamber, D: Extraction Chamber, NS: Normal Saline. V1–V3 are pneumatic valves. E1–E4 are four pairs of electrodes.

the input volume of normal saline and measures the volume of transdermally extracted ISF via the time for the electrolytic fluid to establish electrical connection between electrodes while it is transferred between chambers. The defined volume of normal saline between valve V3 and electrode pair E3, shown as the red curve in Figure 2, is transferred into the extraction chamber by detecting the resistance of electrode pair E3 and changing the status of pneumatic valves. And the volume of collected ISF sample, shown as the blue curve in Figure 2, can be calculated as follows:

$$V = V_C + \frac{1}{2}WH(t_4 - t_1) \left(\frac{S}{t_1 - t_2} + \frac{S}{t_3 - t_4} \right), \quad (1)$$

where V_C is the volume of the microchannel between electrode pair E1 and E4, W and H are the width and height of the microchannel, t_1 and t_2 are the time for the head of sample flowing through the electrode pair E1 and E2, t_3 and t_4 are the time for the tail of sample flowing through the electrode pair E3 and E4, and S (10 mm) is the distance between two pairs of electrodes. The volume of transdermally extracted ISF equals to the difference between the sample volume and the defined input volume of normal saline.

B. Fabrication process of microfluid chip with volume sensor

1. Process for micromolding the polydimethylsiloxane (PDMS) layers

- (a) *SU-8* 100 (MicroChem) was spun on a bare 100 mm silicon wafer. The *SU-8* was subsequently lithographically patterned to form molds of the desired geometry.
- (b) PDMS (SylgardTM 184, Dow Corning) was mixed in a 10:1 ratio of PDMS base with curing agent. After degas sing in the vacuum jar for 45 min, the PDMS was poured onto *SU-8* molds.
- (c) The PDMS layers cured at 80 °C for one hour and were then peeled from the molds.

2. Process for fabricating the electrodes layer

- (a) Kapton tape adhering to the aluminum plate was cut by a laser (VersaLASER VLS 3.50). The electrode parts were then peeled from the aluminum plate.
- (b) Kapton tape remaining on the aluminum plate was cleaned in an ultrasonic bath and transferred to a 100 mm glass wafer.
- (c) Ag microparticles were mixed with PDMS in a 4:1 weight ratio to form conductive PDMS.
- (d) After the conductive PDMS was plastered onto the Kapton tape, the Kapton tape was carefully peeled from the glass wafer and the conductive PDMS electrodes were left on the surface of the glass wafer.
- (e) The conductive PDMS electrodes were cured at 80 °C for 1 h, and PDMS was then poured onto the surface of the glass wafer.
- (f) The PDMS layer cured at 80 °C for 1 h and was then peeled from the glass wafer to obtain the electrodes layer.

3. Process for integrating volume sensor

The microchannel layer with a curved microfluidic channel (height: 213 μm, width: 725 μm), the PDMS layer containing four pairs of conductive PDMS electrodes on its surface were bonded together to compose a volume sensor. And the bottom PDMS layer was bonded with the volume sensor together using oxygen plasma (900 mTorr O₂, 25 W, 25 s). There is one short channel on the lower surface of the bottom layer. The bigger hole on bottom layer was utilized as the extraction chamber which was attached on the skin surface. The smaller hole and the short channel were used to connect the extraction chamber and the microchannel layer of the system. Prior to the bonding procedure, the vertical interconnecting channels, the

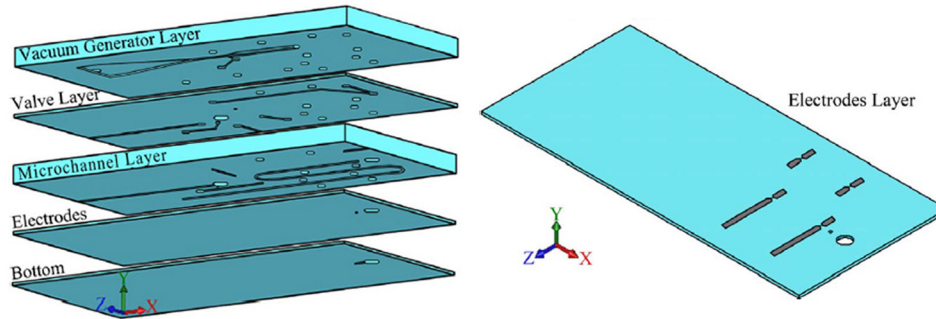


FIG. 3. Schematic of the microfluidic chip with a volume sensor.

electrical connection holes, the connecting ports, and the extraction chamber were drilled and punched in the three layers.

The schematic of the microfluidic chip with a volume sensor is shown in Figure 3.

IV. DESIGN AND FABRICATION OF FIBER SPR SENSOR FOR GLUCOSE MONITORING

A schematic of the fiber-optic SPR sensor is shown in Figure 4. After a white light source is coupled into the optical fiber core, it produces the internal total reflection with different reflection angles θ , and propagates forward. At the same time, the evanescent wave is generated,¹⁰ of which the electric field intensity decays exponentially at the interface between the core and the metal film. And then the collective oscillation of plasmon on the surface of the metal film is excited, generating the surface plasmon wave. When the horizontal component of evanescent wave vector is equal to the surface plasmon wave vector at the interface between gold film and glucose solution, surface plasmon resonance occurs, resulting in a sharp attenuation of the reflected light energy. At that time, the total reflection coefficient (reflectivity) of fiber-optic SPR (FO-SPR) reaches the minimum where the wavelength is called resonance wavelength. It is extremely sensitive to the changes of glucose solution concentration (refractive index) on the surface of a gold film. So the changes of resonance wavelength indicate different glucose concentrations.

A. Structure design of fiber SPR sensor

The parameters of the sensor, including the diameter of the fiber core D , the length of the optic fiber sensing region L , the thickness of the gold film d_1 , and the thickness of the chromium layer d_2 , were simulated and analyzed using Matlab based on FO-SPR principles¹¹ to reasonably design the structure of the sensor and to optimize its performance. The relation between the total reflection coefficient and the wavelength of the incident light is merely related to the remaining parameter when three parameters are fixed. In these SPR curves, the accuracy

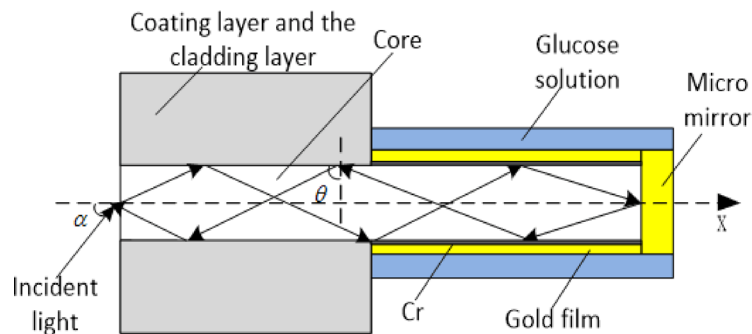


FIG. 4. Schematic of the fiber-optic SPR sensor for glucose concentration measurement.

of the spectral analysis is higher when the attenuation depth is deeper and the Full Width at Half Maximum (FWHM) is narrower.

1. The fiber core diameter

In this simulation, the thicknesses of the gold film and the chromium layer are 50 nm and 5 nm, respectively, and the length of the sensing region is 10 mm. As shown in Figure 5(a), as the fiber core diameter increases from 62.5 μm to 600 μm , the reflectivity and the attenuation depth of the SPR curve increase, and the FWHM decreases, while the resonance wavelength is almost unchanged. However, the core diameter should not be too large because an optical fiber with a larger core diameter has more dispersion and a lower optical bandwidth. Considering that customization is needed when the core diameter is less than 600 μm , 600 μm was chosen as the core diameter.

2. The length of the sensing region

The reflectivity curves of the sensor were obtained through the simulation for thicknesses of the chromium layer and the gold film of 5 nm and 50 nm, respectively, a fiber core diameter of 600 μm , and the length of sensing region in the range from 5 mm to 30 mm. The reflectivity decreases and the attenuation depth of SPR curve increases as the length of the sensing region increases in Figure 5(b). The sensitivity decreased when the sensing region length was increased. To balance the attenuation depth and the sensitivity,¹² 15 mm was chosen as the length of the sensing region.

3. The thickness of the chromium layer

The fiber core diameter is 600 μm , the length of the sensing region is 15 mm, and the gold film thickness is 50 nm in this simulation. The reflectivity curves obtained from the analysis

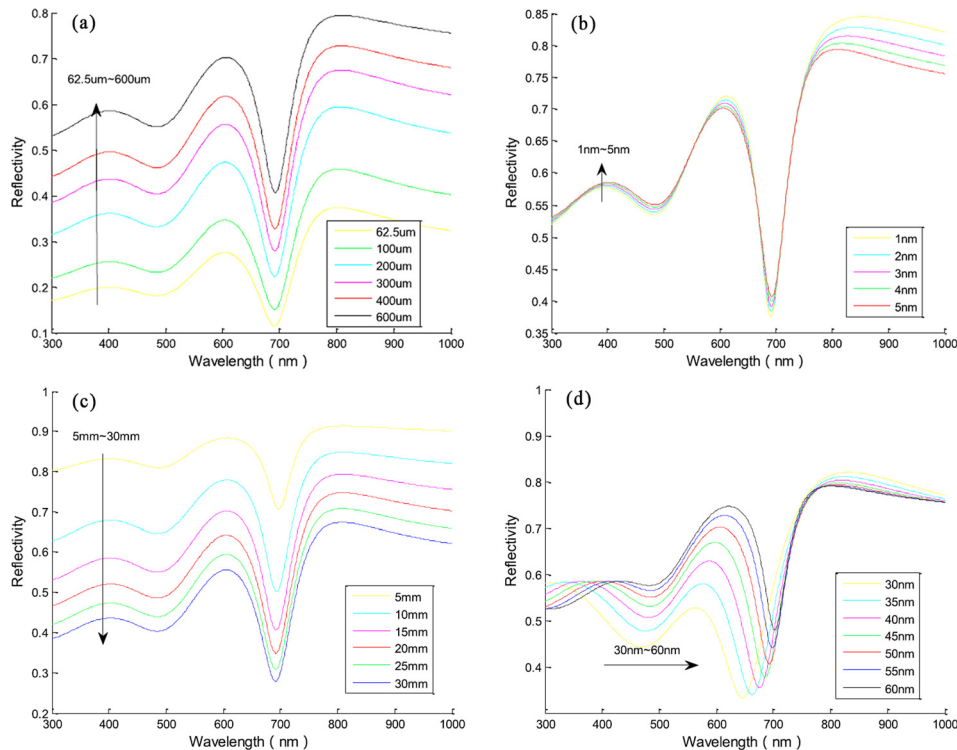


FIG. 5. (a) Simulation of the fiber core diameter, (b) simulation of the sensing region length, (c) simulation of chromium layer thickness, and (d) simulation of gold film thickness.

and calculation are shown in Figure 5(c). The simulation results show that the changes of the chromium thickness have little effect on the attenuation depth and the FWHM of the sensor as well as the sensitivity. Considering that it is easier to control the thickness precisely in the coating process when the metal film is thicker, 5 nm was chosen as the optimal value of the chromium layer thickness.

4. The thickness of the gold film

A fiber core diameter of 600 μm , a sensing region length of 15 mm, and a chromium layer thickness of 5 nm were fixed. We obtained the reflectivity curves of the sensor by changing the gold thickness. As shown in Figure 5(d), the SPR curve has a red shift and the FWHM decreases when the gold thickness increases; meanwhile, the attenuation depth increases and then decreases, and the sensitivity increases. Therefore, to enhance the accuracy of the spectral analysis and to accurately control the film thickness during fabrication, 50 nm was chosen as the gold film thickness.

B. Fabrication process of fiber SPR sensor

The fabrication process of the FO-SPR sensor includes pretreatment of the optical fiber, vacuum coating of the end surface of the fiber core with a 5 nm chromium layer and a 300–400 nm gold film to form the micro mirror structure for light reflection, and vacuum coating of the cylindrical surface of the fiber core with a 5 nm chromium layer and a 50 nm gold film to form the sensing region. A multimode fiber with a 600 μm core diameter was stripped of the coating and cladding layers for a 15-mm section at one end. Then, the end surface and the cylindrical surface of the fiber core to be coated was polished, cleaned with alcohol in an ultrasonic bath, and rinsed with deionized water to ensure the cleanliness and a smooth surface for vacuum coating. Coating the end surface of the multimode fiber with a dense homogeneous metal layer was difficult because of the small area of the fiber core with a 600 μm diameter. Two pieces of glass slide were used to constitute a unified smooth plane together with the end surface. The plane was polished before insertion into the clamping mechanism.

It is also a significant challenge to coat the cylindrical surface of the multimode fiber core uniformly during the vacuum evaporation process. A method is proposed wherein the fiber is rotated in addition to the revolution of the coating disc in the vacuum coating machine. The cylindrical surface of the fiber core to be coated was exposed through the square hole of the coating disc as shown in Figure 6, and metal vapor could be evaporated onto the fiber through the square hole from the inside direction. The rotation of the fiber and the revolution of the coating disc were combined in the vacuum coating machine to achieve a uniform coating. The end face of fiber core was polished and coated with chromium (5 nm) as well as gold (300 nm) successively to form the micro-mirror which was only used to reflect lights. Then, chromium (5 nm) and gold (50 nm) were deposited on the bare cylindrical surface of the fiber core. This was the sensing region. After the coating process, an SMA905 connector was installed. Finally, the FO-SPR sensor was inserted into a microchannel of the microfluid chip.

V. EXPERIMENTAL METHOD AND SYSTEM

In order to verify the performance of the system consisted of LOC based on ISF extraction and fiber SPR glucose sensor, glucose solutions with different concentration were utilized to simulate the interstitial fluid. The pigskin was pretreated by the low-frequency ultrasonic to increase the permeability. The PDMS lab on chip system was put on the preprocessed pigskin to extract the “ISF analogue” under the pigskin transdermally with vacuum.¹³ Considering the complexity of human ISF, as some works of our group, borate polymer which was bond onto the gold surface with layer-by-layer method was utilized to specially adsorb the glucose molecule.¹⁴ When the glucose concentration increased, more glucose molecule will be adsorbed on it. When it decreased, some molecules will dissociate from the polymer and go back to the solution. SPR measurement is exactly based on the changes of the solution refractive index. Thus,

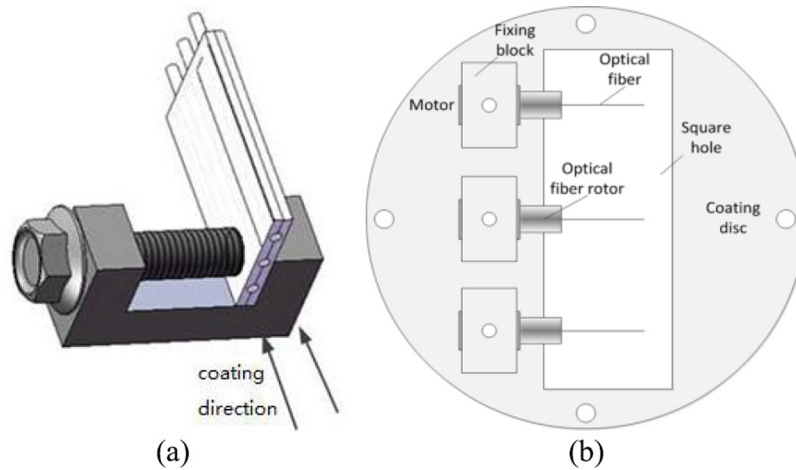


FIG. 6. Clamping mechanisms of FO-SPR sensor coating. (a) Clamping mechanism for the end surface coating. (b) Clamping mechanism for the circumferential surface coating.

the refractive index changes of the SPR sensor with borate polymer were only caused by the different glucose concentrations. But this paper focuses on the integration of LOC system based ISF extraction, volume sensor, and SPR glucose sensor. In order to verify the performance of the whole microsystem quickly, the glucose solution was used to simulate the ISF extracted transdermally. The -6 kPa vacuum pressure generated from the Venturi tube was used to manipulate the fluid flow in the microfluidic system. The status of the pneumatic valve was determined by the pressure on the top of its membrane through computer programmed solenoid valve. With 1 kHz sampling rate, the resistance of electrode pairs was monitored through a data acquisition interface (NI USB-M6251), which was also used to control the status of the solenoid valves, in three steps: the normal saline injection step (E3), the ISF volume measurement step (E1-E4), and the glucose concentration measurement step (E5-E6). The experimental setup for glucose concentration measurement is shown in Figure 7. The light emitted from Halogen light source (Ocean Optics, HL-2000) was coupled into a Y-type optical fiber coupler. And through trunk 3, it entered the SPR sensor placed in glucose solution, then reached to the spectrometer (Ocean Optics, USB2000) along the trunk 3 and branch 2 after the reflection of micro-mirror which is a part of the sensor. Finally, the data were sent from the spectrometer to a computer for signal analysis to get SPR curve.

VI. RESULTS AND DISCUSSION

A simulation experiment was performed to test the functionalities of the optical lab-on-a-chip system. A defined volume ($9.50\text{ }\mu\text{l}$) of normal saline was first inputted into the extraction

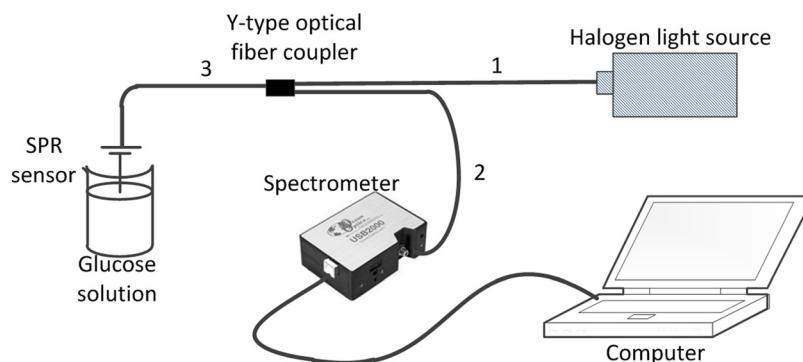


FIG. 7. Schematic of the experimental setup for fiber optic SPR sensor to measure glucose concentration.

TABLE I. Volume sensor test results.(Defined input volume: 9.50 μl , five trials each. All units are in μl .)

Injected volume	Mixture volume	Standard deviation	Volume increment	Absolute error
0.00	9.497	0.048	0.000	0.000
0.40	9.884	0.036	0.387	0.013
0.80	10.309	0.030	0.812	0.012
1.20	10.738	0.025	1.242	0.042
1.60	11.113	0.045	1.617	0.017
2.00	11.474	0.040	1.977	0.023

chamber under the control of the volume sensor. It mixed with an “ISF analogue” which was injected into the extraction chamber by a microsyringe to simulate the transdermally extracted ISF. Then the volume and glucose concentration of the mixture were measured while it was collected from the extraction chamber to the collection chamber, and measured using the flow sensor. Six different volumes from 0 to 2 μl were tested in fixed increments of 0.4 μl to simulate varied ISF volumes. For each “ISF analogue” volume, the simulated ISF volume test was repeated five times.

The flow sensor test results of simulated ISF volume measurements are shown in Table I. The standard deviation for every sample is less than 0.05 μl , and the absolute error of added volume (to simulate the transdermally extracted ISF volume) measurements is less than 0.042 μl . Specifically, when the added volume is no more than 0.8 μl , the absolute error is less than 0.013 μl , which indicates a strong relationship between the volume measured by the flow sensor and the extracted ISF volume.

The relationship between glucose concentration and the resonance wavelength was shown in Figure 8. The R-square of the fitting curve is 0.9558, and the resonance wavelength moves from 549.081 nm to 592.914 nm while the concentration ranges from 0 to 200 mg/dl. We also selected three different concentrations (100 mg/dl, 150 mg/dl, and 200 mg/dl) to verify the repeatability of the system by ten times measurements of each concentration. The fitting curve in Figure 9 showed the good repeatability of the sensor, which has the max error value 1.1 nm and the min value 0.2 nm.

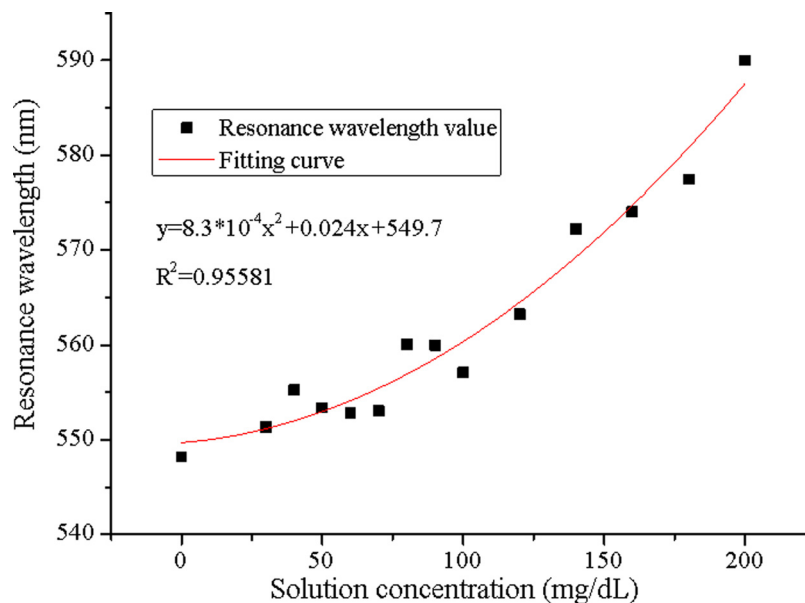


FIG. 8. Solution concentration measurement experiments.

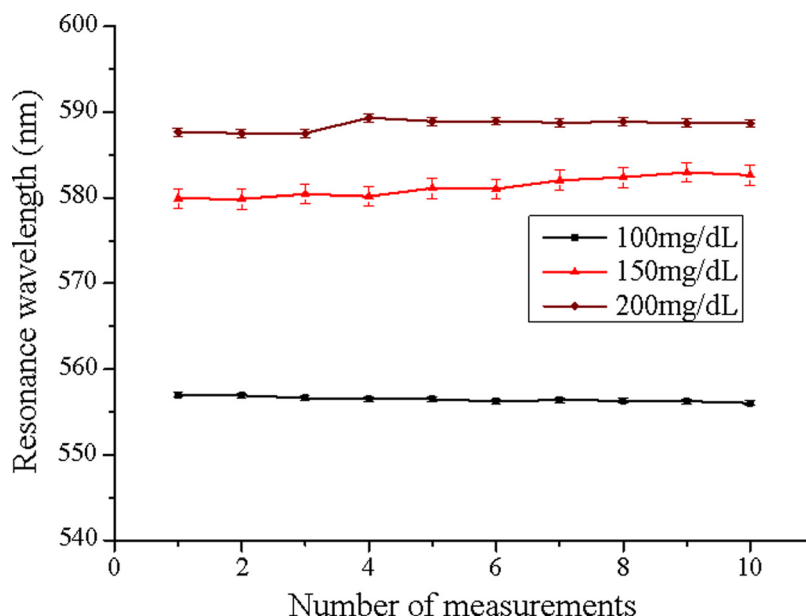


FIG. 9. Repeatability and reproducibility experiments.

VII. CONCLUSION

A lab-on-a-chip system is proposed for ISF transdermal extraction, volume measurement, and optical glucose sensing towards the application of continuous glucose monitoring. This device mainly contains a MEMS volume sensor which measures extracted ISF volume via conductance monitoring and a fiber SPR glucose sensor which measures glucose concentrations in the transdermally extracted ISF. A simulating test of ISF collection, volumetric measurement, and glucose sensing is done with the device. Six different volumes from 0–2 μl in fixed increments of 0.4 μl were tested. The standard deviation for every sample is less than 0.05 μl , and the absolute error of added volume measurements is less than 0.042 μl . The relationship between glucose concentration and the resonance wavelength was shown in Figure 8. The R-square of the fitting curve is 0.9558, and the resonance wavelength moves from 549.081 nm to 592.914 nm while the concentration ranges from 0 to 200 mg/dl. We also selected three different physiological glucose concentrations (100 mg/dl, 150 mg/dl, and 200 mg/dl) to verify the repeatability of the system by ten times measurements of each concentration. The fitting curve showed the good repeatability of the sensor, which has the max error value 1.1 nm and the min value 0.2 nm. The experiment results showed that this method could detect different glucose concentrations (0–200 mg/dl) with good repeatability and will be suitable for glucose monitoring in clinical application.

ACKNOWLEDGMENTS

This work was supported by the National Natural Science Foundation of China (Grant Nos. 61428402 and 81571766), the Key Projects in the Science & Technology Pillar Program of Tianjin (Grant No. 11ZCKFSY01500), the Key Projects of Tianjin Natural Science Foundation Program (Grant No. 15JCZDJC36100), the National High Technology Research and Development Program of China (Grant No. 2012AA022602), and the 111 Project of China (Grant No. B07014).

¹D. A. Gough and T. Bremer, *Diabetes Technol. Ther.* **2**(3), 377 (2000).

²J. Okuda, J. Wakai, N. Yuhashi, and K. Sode, *Biosens. Bioelectron.* **18**(5–6), 699 (2003).

³J. Wang, *Chem. Rev.* **108**(2), 814 (2008).

⁴J. H. Zhu, Z. Q. Zhu, Z. S. Lai, R. Wang, X. M. Guo, X. Q. Wu, G. X. Zhang, Z. R. Zhang, Z. R. Zhang, Y. T. Wang, and Z. Y. Chen, *Sensors* **2**(4), 127 (2002).

- ⁵D. Deis, J. Bolinder, J. P. Riveline, T. Battelino, E. Bosi, N. Tubiana-Rufi, D. Kerr, and M. Phillip, *Diabetes Care* **29**(12), 2730 (2006).
- ⁶S. Weinzimer, D. Xing, M. Tansey, R. Fiallo-Scharer, N. Mauras, T. Wysocki, R. Beck, W. Tamborlane, K. Ruedy, and Diabetes Research in Children Network (DirecNet) Study Group, *Pediatr. Diabetes Care* **31**(3), 525 (2008).
- ⁷J. Kost, S. Mitragotri, R. A. Gabbay, M. Pishko, and R. Langer, *Nat. Med.* **6**(3), 347 (2000).
- ⁸H. Yu, R. C. Roberts, D. Li, K. Xu, and N. C. Tien, Presented at the 5th IEEE International Conference on Nano/Micro Engineered and Molecular Systems (NEMS) (2010).
- ⁹H. Yu, J. Liu, T. Shi, D. Li, Z. Du, and K. Xu, Presented at the Biomedical Optics (BiOS) (2008).
- ¹⁰B. Lee, S. Roh, and J. Park, *Opt. Fiber Technol.* **15**(3), 209 (2009).
- ¹¹D. Z. Stupar, J. S. Bajic, M. P. Slankamenac, L. M. Manojlovic, A. V. Joza, M. G. Jelic, and M. B. Zivanov, in *20th Telecommunications Forum (Telfor)* (2012), p. 939.
- ¹²A. K. Sharma and B. D. Gupta, *Opt. Commun.* **245**(1–6), 159 (2005).
- ¹³H. X. Yu, D. C. Li, R. C. Roberts, K. X. Xu, and N. C. Tien, *J. Microelectromech. S* **21**(4), 917 (2012).
- ¹⁴D. Li, J. Wu, P. Wu, Y. Lin, Y. Sun, R. Zhu, J. Yang, and K. Xu, *Sens. Actuators B: Chem.* **213**, 295 (2015).